Temperature-strain phase diagram for $BaTiO_3$ thin films

Y. L. Li
Department of Materials Science and Engineering, The Pennsylvania State University, University Park, Pennsylvania 16802 and MST-STC, MS K763, Los Alamos National Laboratory, Los Alamos, New Mexico 87545

L. Q. Chen
Department of Materials Science and Engineering, The Pennsylvania State University, University Park, Pennsylvania 16802

(Received 2 June 2005; accepted 18 November 2005; published online 14 February 2006)

The shifts of ferroelectric phase transition temperatures and domain stabilities of $BaTiO_3$ thin films as a function of strain and temperature were studied using phase-field simulations. A new Landau-Devonshire thermodynamic potential based on an eighth-order polynomial was employed for describing the bulk free energy of $BaTiO_3$ single crystals, which allows the exploration of domain stability in the full range of experimentally accessible compressive and tensile strains. Based on the simulation results, a phase diagram was constructed, which displays the stability of various ferroelectric phases and domain structures as a function of temperature and strain. © *2006 American Institute of Physics*. [DOI: 10.1063/1.2172744]

Due to their potential applications in electronic and optical devices, epitaxial ferroelectric thin films have been extensively studied in the last decade both theoretically and experimentally.[1–13] There are convincing experimental evidences that the strain due to lattice and/or thermal expansion mismatch between a film and a substrate may result in dramatic increases in phase transition temperatures as well as large variations of domain structures. For example, it was recently discovered that the cubic to tetragonal ferroelectric transition temperature of epitaxial $BaTiO_3$ thin films could be increased by as much as 500 °C higher than its corresponding bulk by a biaxial compressive substrate strain.[12,14]

It has been shown that such shifts in ferroelectric phase transition temperatures in epitaxial thin films can be predicted using the Laudau-Devonshire phenomenological thermodynamic theory.[4,11,15] However, all existing thermodynamic analysis of phase transitions and domain structures in $BaTiO_3$ thin films is limited to small compressive strains as the existing thermodynamic potential is not applicable to compressive strains larger than ~0.4%.[4,11,15] On the other hand, epitaxial $BaTiO_3$ thin films can be subject to compressive strains as large as 1.6%, i.e., way beyond the 0.4% limit. Furthermore, it is rather difficult to take the domain structure into account in thermodynamic analysis, and as a result, different versions of temperature-strain stability diagrams for $BaTiO_3$ thin films have been published depending on the assumption or approximations of domain states, e.g., single domains for different ferroelectric phases or simplified two-dimensional domain structures.[4,15,16] Prior works on $PbTiO_3$ thin films demonstrated that thermodynamic analysis assuming a single-domain state for each ferroelectric phase or simplified domain structures under different constraints may produce quantitatively inaccurate or sometime qualitatively incorrect domain stability diagrams.[17] Therefore, the main objective of this letter is to employ a newly developed thermodynamic model that is applicable to both large compressive and tensile strains and construct a domain stability diagram for $BaTiO_3$ thin films without *a priori* assumptions on the possible domain structures that might appear at a given temperature and strain. The domain stability diagram is expected to contribute to the design of desirable domain structures of epitaxial $BaTiO_3$ thin films by choosing appropriate substrates and substrate orientations.

Similar to $PbTiO_3$, the phase-field approach is employed to construct a phase diagram for constrained $BaTiO_3$ films. Consider an $(001)_p$-orientated $BaTiO_3$ thin film on a substrate, where the subscript p refers to the pseudocubic Miller index. A rectangular coordinate system, $\mathbf{x}=(x_1,x_2,x_3)$ is set up with the x_1, x_2, and x_3 axes along the $[100]_p$, $[010]_p$ and $[001]_p$ crystallographic directions of the cubic $BaTiO_3$ film. The spatial distribution of spontaneous polarization $\mathbf{P}=(P_1,P_2,P_3)_p$ describes the ferroelectric domain structure. The temporal evolution of the polarization $\mathbf{P}$ and thus the domain structures are described by the time dependent Ginzburg-Landau (TDGL) equations,

$$\frac{\partial P_i(\mathbf{x},t)}{\partial t} = -L\frac{\delta F}{\delta P_i(\mathbf{x},t)}, \quad (i=1,2,3), \tag{1}$$

where L is the kinetic coefficient, and F is the total free energy of the system. $\delta F/\delta P_i(\mathbf{x},t)$ is the thermodynamic driving force for the spatial and temporal evolution of $P_i(\mathbf{x},t)$. The total free energy includes the bulk free energy, elastic deformation energy, dipole-dipole interaction energy, and domain wall energy, i.e.,

$$F = \int\int\int_V [f_{\text{bulk}}(P_i) + f_{\text{elas}}(P_i,\varepsilon_{ij}) + f_{\text{elec}}(P_i,E_i) + f_{\text{wall}}(P_{i,j})]d^3x, \tag{2}$$

where V is the volume of the film and $d^3x=dx_1dx_2dx_3$. We assume that the strain field ε_{ij} and electric field E_i are always at equilibrium for a given polarization field distribution.

The bulk free energy density under a stress-free boundary condition is described by an eighth-order Landau-Devonshire polynomial,

$$f_{\text{bulk}} = \alpha_1(P_1^2+P_2^2+P_3^2) + \alpha_{11}(P_1^4+P_2^4+P_3^4) + \alpha_{12}(P_1^2P_2^2 + P_2^2P_3^2+P_1^2P_3^2) + \alpha_{111}(P_1^6+P_2^6+P_3^6) + \alpha_{112}[P_1^2(P_2^4 + P_3^4) + P_2^2(P_1^4+P_3^4) + P_3^2(P_1^4+P_2^4)] + \alpha_{123}P_1^2P_2^2P_3^2 + \alpha_{1111}(P_1^8+P_2^8+P_3^8) + \alpha_{1112}[P_1^6(P_2^2+P_3^2) + P_2^6(P_1^2 + P_3^2) + P_3^6(P_1^2+P_2^2)] + \alpha_{1122}(P_1^4P_2^4+P_2^4P_3^4+P_1^4P_3^4) + \alpha_{1123}(P_1^4P_2^2P_3^2+P_2^4P_3^2P_1^2+P_3^4P_1^2P_2^2), \quad (3)$$

where the coefficients α_1, α_{ij}, α_{ijk}, and α_{ijkl} are fitted to single crystal properties.[18,19]

The elastic energy density is given by

$$f_{\text{elas}} = \tfrac{1}{2}c_{ijkl}e_{ij}e_{kl} = \tfrac{1}{2}c_{ijkl}(\varepsilon_{ij}-\varepsilon_{ij}^0)(\varepsilon_{kl}-\varepsilon_{kl}^0), \quad (4)$$

where c_{ijkl} is the elastic stiffness tensor, $e_{ij}=\varepsilon_{ij}-\varepsilon_{ij}^0$ is the elastic strain, ε_{ij} is the total strain, and ε_{ij}^0 is the stress-free strain or transformation strain. Both ε_{ij} and ε_{ij}^0 are defined using the cubic phase as the reference and $\varepsilon_{ij}^0=Q_{ijkl}P_kP_l$ where Q_{ijkl} represents the electrostrictive coefficient. The summation convention for the repeated indices is employed and $i,j,k,l=1,2,3$. The solution to the mechanical equilibrium equations for a film-substrate system[17,20] is obtained using a combination of the Khachaturyan's mesoscopic elasticity theory[21,22] and the Stroh formalism of anisotropic elasticity.[23,24]

The electrostatic energy of a domain structure is

$$f_{\text{elec}} = -\tfrac{1}{2}E_iP_i, \quad (5)$$

where the electric field E_i depends on the polarization distribution and the electric boundary conditions.[25,26]

The domain wall energy is introduced through the gradients of the polarization field. For a general anisotropic system, the gradient energy density may be represented as

$$f_{\text{wall}} = \tfrac{1}{2}G_{ijkl}P_{i,j}P_{k,l}, \quad (6)$$

where $P_{i,j}=\partial P_i/\partial x_j$ and G_{ijkl} is the gradient energy coefficients with the property of $G_{ijkl}=G_{klij}$. For an isotropic system, it degenerates to

$$f_{\text{wall}} = \tfrac{1}{2}G_{11}(P_{1,1}^2+P_{1,2}^2+P_{1,3}^2+P_{2,1}^2+P_{2,2}^2+P_{2,3}^2+P_{3,1}^2 + P_{3,2}^2+P_{3,3}^2), \quad (7)$$

where G_{ij} is related to G_{ijkl} through the Voigt's notation, for instance, $G_{11}=G_{1111}$.

The temporal evolution of the polarization, and thus the domain structures, are obtained by numerically solving Eq. (1) using the semi-implicit Fourier-spectral method.[27] A model size of $128\Delta x\times 128\Delta x\times 36\Delta x$ was employed, and periodic boundary conditions were applied along the x_1 and x_2 axes. Δx is the grid spacing. The thickness of the film is taken as $h_f=20\Delta x$. The region of the substrate allowed to deform was assumed to be $h_s=12\Delta x$. Our simulations showed little change in results when h_s exceeds about half of the film thickness.[17] The elastic constants and electrostrictive coefficients employed in the simulations are listed in Ref. 18.[28–30] Due to the lack of experimental data, isotropic domain wall energy was assumed and $G_{11}/G_{110}=1.0$ where G_{110} is related to the magnitude of Δx through $\Delta x=\sqrt{G_{110}/\alpha_0}$ and $\alpha_0=|\alpha_1|_{T=25\,^\circ\text{C}}$. We performed a number of simulations by assuming different degrees of domain wall energy anisotropy. It is shown that the domain wall energy anisotropy does not have a significant effect on domain morphology and volume fractions. The average strains imposed by the substrate are assumed to be $\bar{\varepsilon}_{11}=\bar{\varepsilon}_{22}=e_0$. The short-circuit surface boundary condition was employed for computing the dipole-dipole interactions.[31]

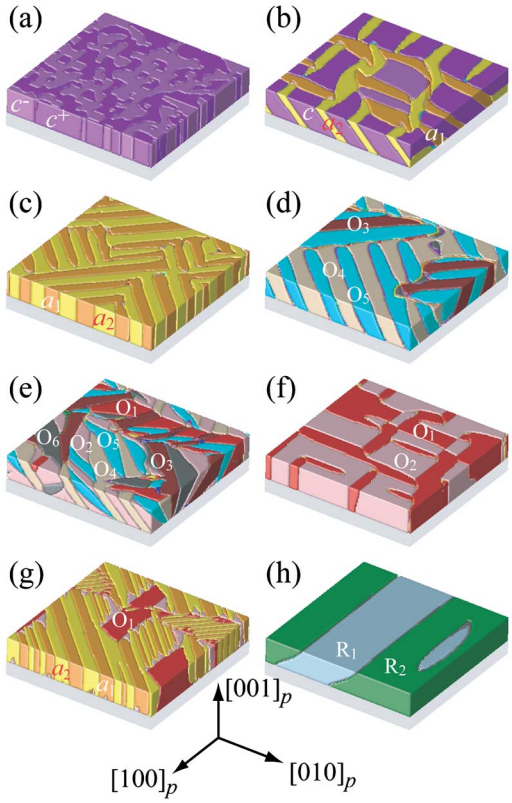

FIG. 1. Domain morphologies in $BaTiO_3$ films as a function of temperature (T) and substrate constraint strain (e_0). Domain definitions and the corresponding polariztions: $a_1:(P_1,0,0)_p$; $a_2:(0,P_1,0)_p$; $c:(0,0,P_3)_p$; $O_1:(P_1,P_1,0)_p$; $O_2:(P_1,-P_1,0)_p$; $O_3:(P_1,0,P_3,)_p$; $O_4:(P_1,0,-P_3)_p$; $O_5:(0,P_1,P_3)_p$; $O_6:(0,P_1,-P_3)_p$; $R_1:(-P_1,-P_1,P_3)_p$; $R_2:(P_1,-P_1,P_3)_p$. (a) phase $\mathbf{T}^F$ at $T=25\,^\circ$C and $e_0=-1.0\%$; (b) phase $\mathbf{T}^F+\mathbf{O}_1^F$ at $T=75\,^\circ$C and $e_0=0.0$; (c) phase $\mathbf{O}_1^F$ at $T=50\,^\circ$C and $e_0=0.2\%$; (d) phase $\mathbf{M}_1^F$ at $T=-25\,^\circ$C and $e_0=-0.05\%$; (e) phase $\mathbf{M}_1^F+\mathbf{O}_2^F$ at $T=-25\,^\circ$C and $e_0=0.1\%$; (f) phase $\mathbf{O}_2^F$ at $T=25\,^\circ$C and $e_0=1.0\%$; (g) phase $\mathbf{O}_1^F+\mathbf{O}_2^F$ at $T=25\,^\circ$C and $e_0=0.25\%$; (h) phase $\mathbf{M}_2^F$ at $T=-100\,^\circ$C and $e_0=0.1\%$.

Examples of domain structures from the simulations are shown Fig. 1. The letters '**T**', '**O**', and '**M**' used in the phase notations indicate 'tetragonal', orthorhombic', and 'monoclinic' crystallographic symmetries, respectively, under a constraint. The superscript 'P' or 'F' tells whether a phase is paraelectric or ferroelectric. '$\mathbf{M}_1^F+\mathbf{O}_2^F$' indicates a mixture of $\mathbf{M}_1^F$ and $\mathbf{O}_2^F$. All the simulations started from a homogeneous paraelectric state with a small random noise of uniform distribution. The domain structures correspond to near equilibrium states, i.e., no significant changes take place with prolonged annealing.

Based on the simulation results, a phase diagram, i.e., a representation of stable ferroelectric phases and domain structures as a function of temperature and strain, is constructed and shown in Fig. 2. Under sufficiently large compressive strains, the ferroelectric phase is of tetragonal symmetry with polarization orthogonal to the film/substrate interface. Figure 1(a) is a typical domain structure under large compressive strains, in which there are two types of c-domains separated by 180° domain walls. This result has been confirmed by experimental measurements on $BaTiO_3$ films commensurately grown on $DyScO_3$ and $GdScO_3$ sub-

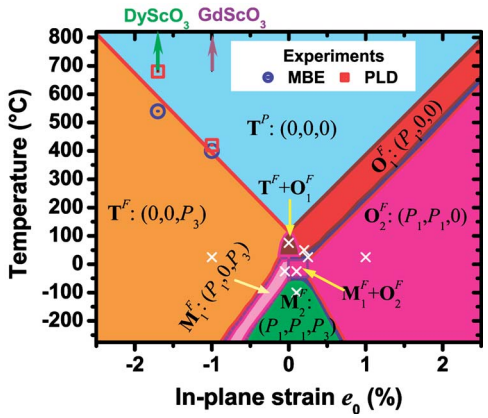

FIG. 2. Phase diagram of $BaTiO_3$ films as a function of temperature and substrate in-plane strain. The scattered circles and squares denote the ferroelectric transition temperatures measured from experiments on the $BaTiO_3$ films commensurately grown on $DyScO_3$ and $GdScO_3$ substrates, respectively (Ref. 12). The × indicates the locations of the domain structures shown in Fig. 1. Each single phase has equivalent variants with polarization vectors of $\mathbf{P}=(0,0,0)_p$ in $\mathbf{T}^P$; $\mathbf{P}=(0,0,\pm P_3)_p$ in $\mathbf{T}^F$; $\mathbf{P}=(\pm P_1,0,0)_p/(0,\pm P_1,0,0)_p$ in $\mathbf{O}_1^F$; $\mathbf{P}=(\pm P_1,\pm P_1,0)_p/(\pm P_1,\mp P_1,0)_p$ in $\mathbf{O}_2^F$; $\mathbf{P}=(\pm P_1,0,\pm P_3)_p/(\pm P_1,0,\mp P_3)_p/(0,\pm P_1,\pm P_3)_p/(0,\pm P_1,\mp P_3)_p$ in $\mathbf{M}_1^F$; $\mathbf{P}=(\pm P_1,\pm P_1,\pm P_3)_p/(\pm P_1,\mp P_1,\pm P_3)_p/(\pm P_1,\pm P_1\mp P_3)_p/(\pm P_1,\mp P_1,\mp P_3)_p$ in $\mathbf{M}_2^F$.

strates through reactive molecular beam epitaxy (MBE) and pulsed-laser deposition (PLD), respectively.[12] Under larger tension strains the polarization of ferroelectric phases is parallel to the film/substrate interface, either along $[100]_p$ or $[110]_p$ direction depending on temperature and the magnitude of strain. The corresponding domain structures are similar to either the $\mathbf{O}_1^F$ twins as shown in Fig. 1(c), or the $\mathbf{O}_2^F$ twins of Fig. 1(f), or the mixture of $\mathbf{O}_1^F$ twins and $\mathbf{O}_2^F$ twins shown in Fig. 1(g). Under relative smaller strains the polarization changes its orientation from $<100>_p$ to $<10\lambda>_p$ then to $<11\lambda>_p$ as temperature decreases. This sequence is similar to that in bulk single crystals but λ is not always equal to 1 as in bulk. The domain variants vary with the in-plane strain, which are clearly shown in Fig. 1(a)–1(c) for the $<100>_p$ orientated polarizations and in Fig. 1(d)–1(f) for the $<10\lambda>_p$ orientated polarizations. The phase diagram indicates that under certain ranges of strains, the ferroelectric phases with both symmetries 4*mm* and *mm*2 can be stable down all the way to 0 K without further transformation. It is interesting to notice that the domain structures with $<10\lambda>_p$ oriented polarizations can be rather complicated: the domain walls between different variants not only along the $\{100\}_p$ and $\{110\}_p$ planes, i.e., the crystallographically prominent walls with a fixed orientation, but also the so-called S-walls,[32] whose orientations depend on the magnitude of the polarization, electrostrictive coefficients and substrate constraint. When the strain is small, its effect on the orientation of orthorhombic domain wall can be ignored. In such a case, the permissible domain walls are either $\{100\}_p$ or $\{110\}_p$ or $\{11\gamma\}_p$ planes with $\gamma=2Q_{44}/(Q_{11}-Q_{12})=0.440299$. This reinforces our prior argument that it is not reliable to construct a domain map assuming single domains or by considering only the crystallographically prominent domain wall orientations.[4,15,16] Similarly, the domain walls between different variants of $\mathbf{M}_2^F$ can be either along the $\{100\}_p$ planes[15] or the $\{110\}_p$ planes of the prototypic cubic phase as shown in Fig. 1(h) as it has been previously discussed.[5,31]

In summary, a phase/domain stability diagram as a function of temperature and substrate constraint strain was constructed for $BaTiO_3$ thin films using a new set of Landau coefficients based on an eighth-order polynomial and phase-field simulations.

The authors are grateful to Dr D. Schlom and Dr. S. Streffer for suggestions and discussions, particularly on the nomenclature and the labeling of the domain stability diagram. This work was supported by the NSF under Grant Nos. DMR-0122638 and DMR-0103354.

[1] J. S. Speck and W. Pompe, J. Appl. Phys. **76**, 466 (1994).
[2] J. S. Speck, A. Seifert, W. Pompe, and R. Ramesh, J. Appl. Phys. **76**, 477 (1994).
[3] C. M. Foster, G. R. Bai, R. Csencsits, J. Vetrone, R. Jammy, L. A. Wills, E. Carr, and J. Amano, J. Appl. Phys. **81**, 2349 (1997).
[4] N. A. Pertsev, A. G. Zembilgotov, and A. K. Tagantsev, Phys. Rev. Lett. **80**, 1988 (1998).
[5] S. K. Streiffer, C. B. Parker, A. E. Romanov, M. J. Lefevre, L. Zhao, J. S. Speck, W. Pompe, C. M. Foster, and G. R. Bai, J. Appl. Phys. **83**, 2742 (1998).
[6] S. P. Alpay and A. L. Roytburd, J. Appl. Phys. **83**, 4714 (1998).
[7] A. L. Roytburd, S. P. Alpay, L. A. Bendersky, V. Nagarajan, and R. Ramesh, J. Appl. Phys. **89**, 553 (2001).
[8] M. Sepliarsky, S. R. Phillpot, M. G. Stachiotti, and R. L. Migoni, J. Appl. Phys. **91**, 3165 (2002).
[9] J. H. Haeni, P. Irvin, W. Chang, R. Uecker, P. Reiche, Y. L. Li, S. Choudhury, W. Tian, M. E. Hawley, B. Craigo, A. K. Tagantsev, X. Q. Pan, S. K. Streiffer, L. Q. Chen, S. W. Kirchoefer, J. Levy, and D. G. Schlom, Nature (London) **430**, 758 (2004).
[10] O. Dieguez, S. Tinte, A. Antons, C. Bungaro, J. B. Neaton, K. M. Rabe, and D. Vanderbilt, Phys. Rev. B **69**, 212101 (2004).
[11] D. A. Tenne, X. X. Xi, Y. L. Li, L. Q. Chen, A. Soukiassian, M. H. Zhu, A. R. James, J. Lettieri, D. G. Schlom, W. Tian, and X. Q. Pan, Phys. Rev. B **69**, 174101 (2004).
[12] K. J. Choi, M. Biegalski, Y. L. Li, A. Sharan, J. Schubert, R. Uecker, P. Reiche, Y. B. Chen, X. Q. Pan, V. Gopalan, L. Q. Chen, D. G. Schlom, and C. B. Eom, Science **306**, 1005 (2004).
[13] B. S. Kang, J. S. Lee, L. Stan, J. K. Lee, R. F. DePaula, P. N. Arendt, M. Nastasi, and Q. X. Jia, Appl. Phys. Lett. **85**, 4702 (2004).
[14] Y. Yoneda, T. Okabe, K. Sakaue, H. Terauchi, H. Kasatani, and K. Deguchi, J. Appl. Phys. **83**, 2458 (1998).
[15] V. G. Koukhar, N. A. Pertsev, and R. Waser, Phys. Rev. B **64**, 214103 (2001).
[16] N. A. Pertsev and V. G. Koukhar, Phys. Rev. Lett. **84**, 3722 (2000).
[17] Y. L. Li, S. Y. Hu, Z. K. Liu, and L. Q. Chen, Acta Mater. **50**, 395 (2002).
[18] $\alpha_1=4.124(T-115)\times10^5$, $\alpha_{11}=-2.097\times10^8$, $\alpha_{12}=7.974\times10^8$, $\alpha_{111}=1.294\times10^9$, $\alpha_{112}=-1.950\times10^9$, $\alpha_{123}=-2.500\times10^9$, $\alpha_{1111}=3.863\times10^{10}$, $\alpha_{1112}=2.529\times10^{10}$, $\alpha_{1122}=1.637\times10^{10}$, $\alpha_{1123}=1.367\times10^{10}$, $c_{11}=1.78\times10^{11}$, $c_{12}=0.964\times10^{11}$, $c_{44}=1.22\times10^{11}$, $Q_{11}=0.10$, $Q_{12}=-0.034$, $Q_{44}=0.029$ (in SI units and T in °C).
[19] Y. L. Li, L. E. Cross, and L. Q. Chen, J. Appl. Phys. **98**, 064101 (2005).
[20] Y. L. Li, S. Y. Hu, Z. K. Liu, and L. Q. Chen, Appl. Phys. Lett. **78**, 3878 (2001).
[21] A. G. Khachaturyan and G. A. Shatalov, Sov. Phys. JETP **29**, 557 (1969).
[22] A. G. Khachaturyan, *Theory of Structural Transformation in Solids* (Wiley, New York, 1983).
[23] A. N. Stroh, J. Math. Phys. **41**, 77 (1962).
[24] T. C. T. Ting, *Anisotropic Elasticity: Theory and Applications* (Oxford University Press, New York, Oxford, 1996).
[25] Y. L. Li, S. Y. Hu, Z. K. Liu, and L. Q. Chen, Appl. Phys. Lett. **81**, 427 (2002).
[26] Y. L. Li, L. Q. Chen, G. Asayama, D. G. Schlom, M. A. Zurbuchen, and S. K. Streiffer, J. Appl. Phys. **95**, 6332 (2004).
[27] L. Q. Chen and J. Shen, Comput. Phys. Commun. **108**, 147 (1998).
[28] A. F. Devonshire, Philos. Mag. **42**, 1065 (1951).
[29] D. Berlincourt and H. Jaffe, Phys. Rev. **111**, 143 (1958).
[30] T. Yamada, J. Appl. Phys. **43**, 328 (1972).
[31] Y. L. Li, S. Y. Hu, and L. Q. Chen, J. Appl. Phys. **97**, 034112 (2005).
[32] J. Fousek and V. Janovec, J. Appl. Phys. **40**, 135 (1969).